Development of functional biointerfaces by surface modification of polydimethylsiloxane with bioactive chlorogenic acid

Ming Wu [a,1], Jia He [b,1], Xiao Ren [c,1], Wen-Sheng Cai [b], Yong-Chun Fang [c], Xi-Zeng Feng [a,*]

[a] State Key Laboratory of Medicinal Chemical Biology, College of Life Science, Nankai University, Tianjin 300071, China
[b] College of Chemistry, Nankai University, Tianjin 300071, China
[c] Institute of Robotics and Automatic Information Systems, Nankai University, Tianjin 300071, China

ABSTRACT

The effect of physicochemical surface properties and chemical structure on the attachment and viability of bacteria and mammalian cells has been extensively studied for the development of biologically relevant applications. In this study, we report a new approach that uses chlorogenic acid (CA) to modify the surface wettability, anti-bacterial activity and cell adhesion properties of polydimethylsiloxane (PDMS). The chemical structure of the surface was obtained by X-ray photoelectron spectroscopy (XPS), the roughness was measured by atomic force microscopy (AFM), and the water contact angle was evaluated for PDMS substrates both before and after CA modification. Molecular modelling showed that the modification was predominately driven by van der Waals and electrostatic interactions. The exposed quinic-acid moiety improved the hydrophilicity of CA-modified PDMS substrates. The adhesion and viability of *E. coli* and HeLa cells were investigated using fluorescence and phase contrast microscopy. Few viable bacterial cells were found on CA-coated PDMS surfaces compared with unmodified PDMS surfaces. Moreover, HeLa cells exhibited enhanced adhesion and increased spreading on the modified PDMS surface. Thus, CA-coated PDMS surfaces reduced the ratio of viable bacterial cells and increased the adhesion of HeLa cells. These results contribute to the purposeful design of anti-bacterial surfaces for medical device use.

© 2013 Elsevier B.V. All rights reserved.

1. Introduction

Bacteria-free devices are universally important for numerous applications that improve human health, such as tissue engineered materials [1], biomedical devices and biosensors. Device-related infections (DRIs), which arise from the adhesion and proliferation of bacteria on the surfaces of biomedical devices and implants, are the significant concern in implant surgery [2]. Thus, the design and fabrication of novel nanostructured surfaces that mitigate bacterial colonisation or inhibit bacterial growth is required to improve current medical devices. Most existing anti-bacterial agents are natural compounds that have been either extracted from microorganisms, such as penicillin, streptomycin and β-lactams [3] or chemically modified. However, the emergence of antibiotic-resistant bacteria is becoming an increasingly serious problem with the abuse of anti-bacterial drugs.

One prominent example is the recent discovery of a metallo-β-lactamase (MBL) named NDM-1 (New Delhi metallo-β-lactamase), which was identified from *Klebsiella pneumoniae* (strain 05-506)

and *Escherichia coli* isolates [4]. Most isolates with the NDM-1 enzyme are resistant to standard intravenous antibiotics [5]. Thus, because of the disadvantages of conventional antimicrobial agents, the development of novel antimicrobial agents has gained considerable attention. For example, Sumitha et al. incorporated silver nanoparticles into poly (ε-caprolactone) (PCL) scaffolds during the process of electrospinning [1]. Eby et al. reported a method to synthesise antimicrobial medical instruments by coating them with silver nanoparticles [6]. "Nanosilver" has been introduced into some consumer products [7] and silver-containing textiles are being advertised for their anti-bacterial effect [8]. Although nanoparticles (NPs) were originally considered nontoxic materials, an increasing number of studies report toxicity associated with NP exposure [9–11]. Therefore, other biocompatible agents should be investigated and developed.

Chlorogenic acid (CA), the ester of cinnamic and quinic acid, is the most abundant hydroxycinnamic acid found in food. Additionally, it is nontoxic [12] and has been shown to inhibit bacterial growth [13]. We used CA to modify the surface of polydimethylsiloxane (PDMS) substrates. PDMS elastomer is of particular interest because it is flexible, easily moulded, nontoxic, optically transparent, gas permeable, inexpensive and chemically inert [14]. Because of these merits, considerable effort has been focused on using PDMS in many applications, such as the development of

antimicrobial materials. Komaromy et al. investigated the effect of changes to the physical properties of PDMS on the attachment and viability of bacterial cells [15]. Goyal et al. demonstrated a method for embedding noble metal NPs in free standing PDMS composite films to synthesise a material with enhanced anti-bacterial properties [16]. Although PDMS has many advantages, its hydrophobic surface restricts its widespread application. Therefore, various solutions have been proposed to improve the hydrophilicity of PDMS surfaces, including plasma oxidation [17], ultraviolet irradiation and adsorbed coatings [18,19]. Although these methods have allowed the tailoring of PDMS surface properties, challenges still remain, including reduced biocompatibility after chemical treatment, hydrophobic recovery and physical damage to the PDMS surface [20,21].

Here, we report a simple approach to modify PDMS with CA (Scheme 1). Our experimental results demonstrate the development of a bi-functional, CA-modified PDMS substrate with increased antimicrobial properties that supports cell growth. These anti-bacterial biomedical devices locally inhibit the growth of bacteria and are not toxic to the surrounding tissue.

2. Materials and methods

2.1. Materials

CA was purchased from Nanjing Zelang Medical Technology Co. Ltd. PDMS elastomer (Sylgard® 184 silicone elastomer kit) was obtained from Dow Corning Corporation (Midland, MI). Propidium iodide (PI) was purchased from Sigma–Aldrich. Other reagents were obtained from Aladdin Reagent Co. Ltd. (China). All of the reagents were of analytical grade. All aqueous solutions were prepared with double-distilled water.

2.2. Preparation of CA-modified PDMS substrates

2.2.1. Preparation of PDMS substrates
PDMS elastomer (Sylgard® 184 silicone elastomer kit) solution is composed of a base (part A) and curing agent (part B). The base and curing agent were mixed in a 10:1 mass ratio, transferred to a glass Petri dish and cured for three days. After being sectioned into discs with a 14-mm diameter, the PDMS substrate was washed with 75% ethanol solution and dried with nitrogen.

2.2.2. PDMS substrate modification with CA
CA solution was prepared in double-distilled water at a concentration of 10 mg mL^{-1}. PDMS substrates were incubated in CA solution for 2 h at ambient conditions. Unattached CA was removed by rinsing the substrate with double-distilled water. The CA-modified PDMS substrates were dried with nitrogen.

2.3. Water contact angle (WCA) measurements

The WCAs of native PDMS and CA-modified PDMS surfaces were determined under ambient conditions using the sessile drop method and an optical contact angle meter (Dataphysics, Inc., OCA20). WCAs were averaged values from ten individual measurements that were collected from different regions on the PDMS surface. All of the measurements were within ±3° of the average. WCAs are presented as the average ± standard deviation.

2.4. X-Ray photoelectron spectroscopy (XPS) measurements

The modification of the PDMS substrate by CA was confirmed by an XPS apparatus (Thermofisher K-Alpha, USA) with a monochromatic Al Kα radiation source. The sample for XPS characterisation was deposited onto a Si slide. XPS analysis was performed on at least

three samples before and after surface modification. The binding energy was swept from 0 to 1350 eV, and the photoelectron take-off angle was set at 45° in fixed analyser transmission mode. The energy resolution of the analyser was 0.9 eV.

### 2.5. Atomic force microscopy (AFM) measurements

The surface morphology of the PDMS substrates was analysed using atomic force microscopy (CSPM 4000, Being-Nano Inc., PR China). The images were scanned in tapping mode in air using commercial Si cantilevers (k = 40 N m^{-1}, Budget Sensors Inc., Bulgaria) with a resonance frequency of 300 kHz. Scan areas of 20 μm × 20 μm and 4.5 μm × 4.5 μm were collected at a 1 Hz scanning rate. Each sample was scanned at five random sites.

2.6. Molecular modelling and dynamics simulations

The coordinates of CA was obtained from the PRODRG server [22], and the conformation is consistent with recent research [23]. The initial structure of the PDMS substrate from our previously published work was used [24]. Briefly, a single PDMS chain consisting of 20 units was equilibrated in the gas phase for 10 ns. Twelve such chains were extracted from the last 2.4 ns of the trajectory and compressed into a slab of 55 Å × 55 Å × 11 Å to construct an amorphous supercell with a density of 0.92 g cm^{-3}. Unbound solid surfaces in the XY plane were modelled using periodic boundary conditions (PBCs). The adsorption of CA was performed using starting structures with their centre of mass (COM) placed >10 Å away from the surface. The assemblies were solvated along the Z-axis to avoid direct contact between CA and the substrate.

All molecular dynamics (MD) simulations were performed using the program NAMD 2.8 [25]. The topology and parameter files for CA were obtained and calculated using the ParamChem website, which is based on the CHARMM36 Generalised Force Field program. The parameters of PDMS were obtained from available literature, and the partial atomic charges were calculated using quantum chemistry [26,27]. The TIP3P water model was employed to model the aqueous solution [28]. PBCs were applied in the three directions of Cartesian space. Long-range electrostatic forces were taken into account using the particle mesh Ewald (PME) method, and a 14-Å cutoff was applied to truncate van der Waals interactions [29]. A temperature of 300 K and a pressure of 1 atm were used to ensure Langevin dynamics and the Langevin piston method [30]. Chemical bonds involving hydrogen atoms were constrained to their experimental lengths by SHAKE/RATTLE algorithms [31,32]. The equations of motion were integrated with a time step of 2 fs. Before production simulation, the molecular system for fixed CA was minimised using up to 5000 conjugate gradient (CG) steps prior to an additional geometry optimisation on the complete interaction using an equal amount of CG steps. A 2 ns MD simulation was subsequently generated with weak harmonic restraints enforced on CA, viz. 1.0 kcal/mol/Å^2. The restraints on CA were removed for the production run. All of the atoms of the PDMS substrate were fixed during the simulation. Visualisation and analysis of the MD trajectories were performed using the VMD program [33].

Because of the chemical inertness of PDMS, adsorption to PDMS usually occurs through physisorption. Therefore, only the initial association of CA with the PDMS substrates was explored. A crucial step in understanding this association is determining the free energy change of adsorption. It was recently demonstrated that the potential of mean force (PMF) is a computationally effective and accurate way to calculate the free energies of interacting substrates and molecules [34–36]. In the present study, PMF profiles that delineated the adsorption process of CA were estimated along the model adsorption pathway, which was defined as the projection onto the Z axis of the distance between the COM of a CA molecule
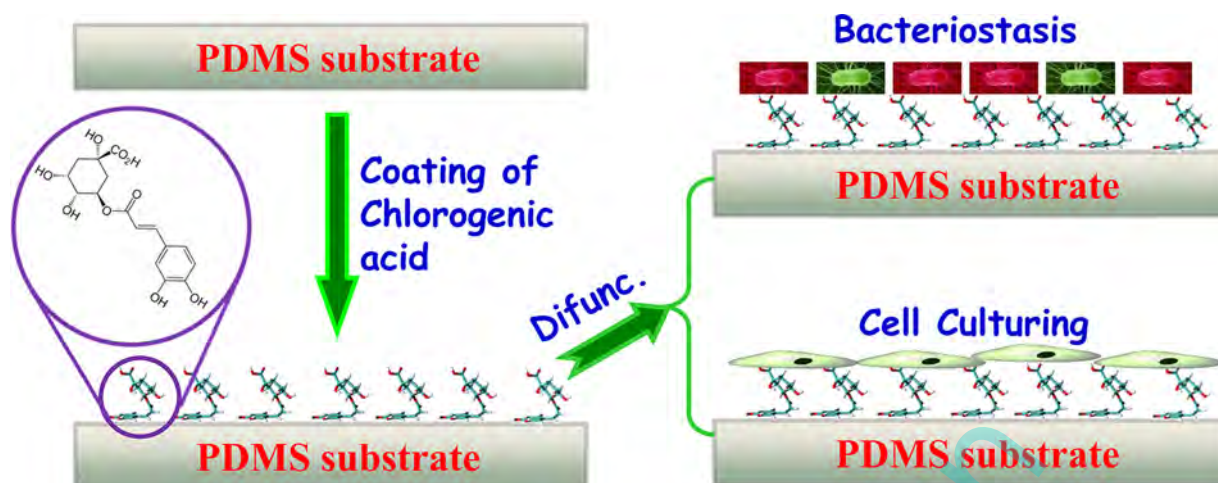
Scheme 1. Schematic depicting the antimicrobial activity and cell growth on CA-modified PDMS surfaces.

and the PDMS surface. To obtain such profiles, the ABF method was implemented using the collective variables module NAMD [37–41]. To increase calculation efficiency, the adsorption pathway was fragmented into consecutive 1-Å wide windows. Instantaneous values of the force were stored in 0.1 Å wide bins. For each of these windows, a trajectory of at least 5 ns long was generated. To improve sample uniformity along the pathway and maintain continuity of the average force across adjacent windows, the width of the windows was adapted as required, and convergence of the free-energy was probed by extending the simulation time for regions featuring energy barriers and minima. The PMF was truncated when inconsistent configurations disrupted sampling uniformity.

2.7. Mechanical test

The mechanical properties of native PDMS and CA-modified PDMS were determined using microcomputer control electron universal testing machines (Jinan Shidai Shijinyiqi Co., Ltd; WDW-05). Rectangular specimens 1.3 mm × 2 mm × 14.5 mm in size were cut from as-prepared products. Six specimens for each group were tested.

2.8. Bacteria culture

Genetically engineered *E. coli* DH5a expressing green fluorescent protein (GFP) was used to investigate the cell density on various substrates. The strain was generously provided by Dr. Jun Feng from the College of Life Science at Nankai University in Tianjin, China. The strain was grown in LB medium at 37 °C with shaking at 150 rpm.

2.9. Antimicrobial activity of CA-modified PDMS substrates

The anti-bacterial activity of CA-coated PDMS was evaluated using the *E. coli* bacterial strain. A comparative study using bare PDMS was the control. The bacterial cells were harvested during exponential growth. To obtain media-free bacteria, cells in the mid-exponential phase were centrifuged and re-suspended in 10 mM phosphate buffer saline (PBS) at pH 7.4 [15,42]. This suspension was added to the CA-coated PDMS substrate.

Both the CA-modified and bare PDMS substrates were cut into 1-cm disks, immersed into the media-free bacterial suspension and incubated for 2 h at room temperature [15]. After incubation, the substrate disks were washed twice with PBS. All experiments were performed under sterile conditions. To determine bacterial cell viability, the CA-coated and uncoated PDMS substrates were soaked in a PI solution (1.5 mM in H_2O) for 15 min. After labelling, substrates were washed with double-distilled water, dried at ambient temperature and visualised with a fluorescent microscope (TE 2000-U Nikon, Japan). Dead cells emitted red fluorescence from the intercalation of PI into the DNA double helix. Viable cells produced green fluorescent protein. Cell viability was evaluated by observing the green or red fluorescence.

2.10. Cell culture on surface-modified PDMS films

The procedure detailed above was also used to prepare unmodified and CA-modified PDMS substrates for cell culture studies. Adhesion and growth experiments were performed with HeLa cells, a human cervical cancer cell line. The substrates were placed in the bottom of 24-well plates. A cell density of 1×10^4 cells cm^{-2} was seeded on the PDMS surfaces, and the substrates were incubated in Dulbecco's modified Eagle's medium (DMEM) with 10% foetal bovine serum at 37 °C and 5% CO_2 for three days. Cell adhesion and growth on the PDMS surfaces were monitored using a Nikon TE2000-U fluorescence microscope with CCD-Rtke (Japan).

3. Results and discussion

3.1. Enhanced hydrophilicity of CA-modified PDMS substrates

Water contact angle (WCA) is an important surface parameter that significantly affects the interaction of proteins and cells with biomaterial surfaces. Cell adhesion and growth is favoured on hydrophilic surfaces [43]. In this study, the wettability of CA-modified PDMS substrates was evaluated by measuring the WCA. As shown in Fig. S1, native PDMS has an average WCA of 104.7° (Fig. S1a), which indicates that the surface of PDMS is reasonably hydrophobic. After modification with CA, the WCA of the PDMS surface decreased to 88.5° (Fig. S1b). Consequently, PDMS surfaces can be modified with CA for improved hydrophilicity. The increased hydrophilicity of the CA-modified PDMS is probably attributed to the three-dimensional structure of the surface. According to Wenzel's law, surface roughness enhances the wetting properties of solid surfaces [44]; smaller WCAs are obtained for surfaces with increased roughness [45]. Another reason for increased PDMS substrate wettability could be attributed to the adherent hydrophilic quinic-acid moiety of CA, which minimises the total energy of the system.
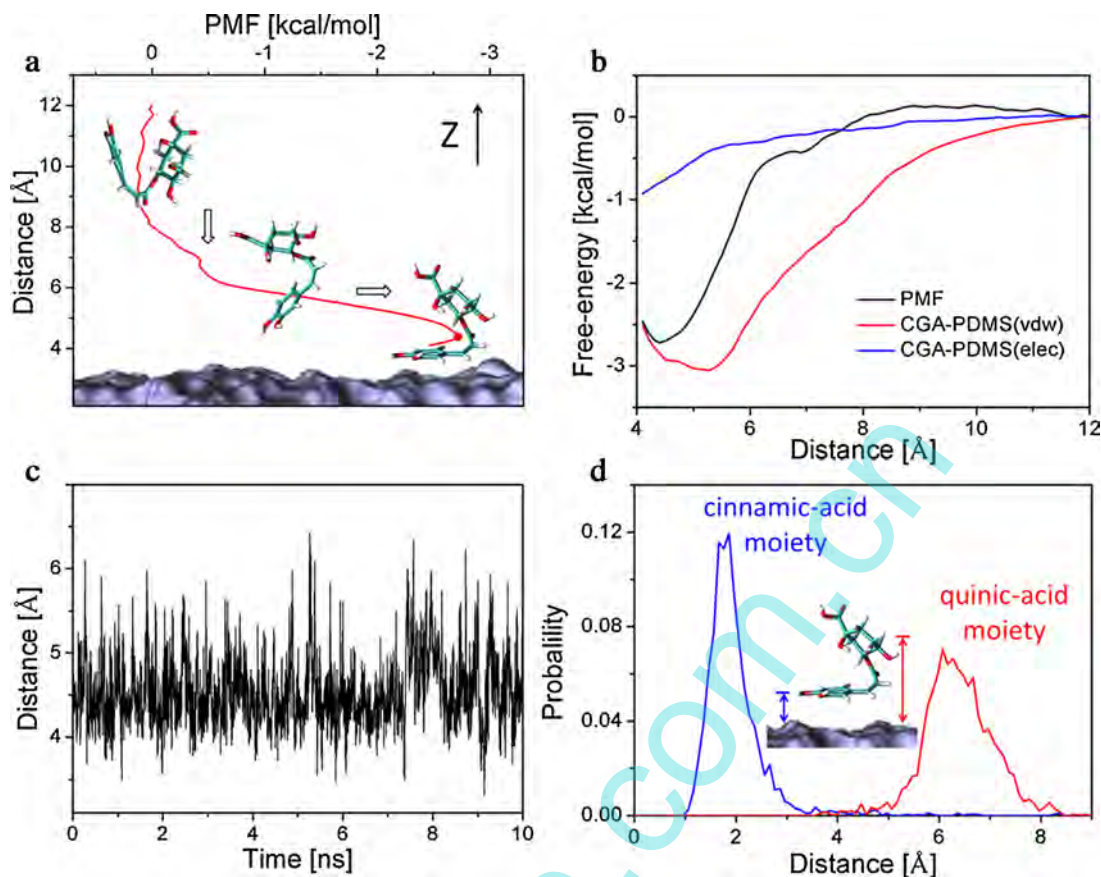
Fig. 1. (a) Free-energy profile along the model adsorption pathway for the adsorption of CA onto the PDMS surface. Inset: representative images from the MD trajectories. (b) Partitioning of the PMF into van der Waals and electrostatic CA-PDMS contributions. (c) Variations in distance between the COM of the CA and the surface of the PDMS substrate during MD simulations. (d) Probability distribution of the distance between the cinnamic acid/quinic acid moiety COM and the surface of the PDMS substrate.

3.2. Chemical characterisation of PDMS surfaces before and after CA modification

The XPS spectra confirmed that the chemical composition of the polymer surface was altered by the CA coating. Fig. S2 presents the full XPS spectra of bare and CA-modified PDMS surfaces on the same scale. The polymer surfaces displayed typical photoelectron peaks for O (1s), C (1s) and Si (2p) (Fig. S2). The results from the XPS analysis for the relative element composition of the substrate surfaces are listed in Table S1. Native PDMS showed the presence of O, C and Si at 23.80, 49.22 and 26.99 atom %, respectively, which is consistent with the expected composition. Successful modification with CA was reflected through the relative element compositions of the substrate surface, which showed an increase in O 1s (from 23.80 to 25.46) and C 1s (from 49.22 to 50.67) and a decrease in Si 2p (from 26.99 to 23.86). Si is only present in the —Si—CH$_3$ group of PDMS; therefore, the decrease in the Si 2p peak indicates coverage of the PDMS surface with CA.

3.3. PDMS surface characterisation using AFM

Surface morphology of the PDMS surface was observed using AFM. We collected AFM images and calculated root mean square (RMS) values. Representative AFM images that illustrate the roughness of the PDMS surface are shown in Fig. 3a and b. The bare PDMS surface was extremely flat (Fig. S3a). After CA modification, the roughness of the PDMS surface increased significantly (Fig. S3b), which indicates that CA adhered to the PDMS surface. RMS values of unmodified and CA-modified PDMS surfaces were 6.904 and 13.33 nm, respectively. The 3D images of these samples validate the

calculated RMS values (Fig. S3a′ and b′). Cell attachment is strongly dependent on surface roughness [46]; cells attach more easily to surfaces with higher roughness values [17].

3.4. Molecular modelling and dynamics simulations

The free-energy profile of the adsorption of CA to the PDMS surface from a given distance was calculated and is shown in Fig. 1a. One global minimum is detected along the adsorption pathway profile, which demonstrates that the binding of CA to the PDMS surface is energetically favourable. In the bound state corresponding to this minimum, the cinnamic-acid moiety adsorbed to the PDMS surface, whereas the quinic-acid moiety interacted with the solvent environment (Fig. S4). Three representative structures of CA were observed along the adsorption pathway, which suggests that the association of CA with the PDMS surface can be represented by a three-stage model. In the diffusion stage, the orientation of the CA molecule was random because CA did not interact with the PDMS substrate. In the association stage, from ~8 to 4.5 Å (corresponding to the bound state), the CA altered its orientation to allow the cinnamic-acid moiety to face and interact with the substrate. During this stage, both van der Waals and electrostatic interactions appear to decrease, as shown in Fig. 1b. This suggests that these forces cooperatively drove adsorption. In the binding stage, there was full contact between the cinnamic-acid moiety and the PDMS surface. The subsequent free-energy barrier predominately resulted from increased repulsive interactions between CA and PDMS. Analysis of the evolution of the solvent-accessible surface area (SASA) of the quinic-acid and cinnamic-acid moiety along the adsorption pathway suggests that the selective interaction in
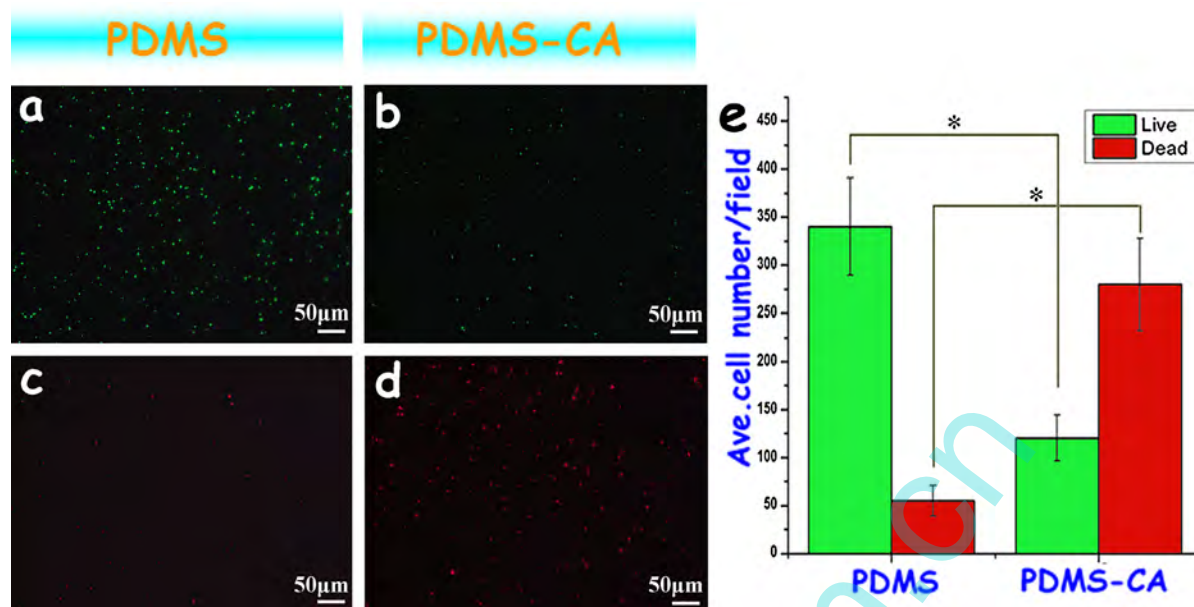
Fig. 2. Anti-bacterial properties of CA-coated PDMS. Fluorescence microscopy images: (a) viable and (b) dead cells on the bare PDMS substrate; (c) viable and (d) dead cells on the CA-coated PDMS substrate; and (e) the number of viable and dead cells was quantified, and the results are presented as the mean ± the standard deviation (SD). *$p < 0.05$ compared with bare PDMS group using Student's *t*-test.

the binding stage is primarily driven by the hydrophobicity of the cinnamic-acid moiety and the hydrophilicity of the quinic-acid moiety (Fig. S5). Additional 10 ns MD simulations were performed to investigate the stability and structural features of CA at the global minima of the free-energy profile. Analysis of the MD trajectories shows that the average distance between CA and the PDMS surface remained roughly constant at approximately 4.5 Å during the entire simulation period (see Fig. 1c), which is consistent with the position of the global minimum in the free-energy landscape. The probability distributions of the distance between the two moieties of CA and the surface were derived from the MD trajectories (see Fig. 1d) and revealed that the hydrophobic cinnamic-acid moiety tended to adhere closely to the surface, whereas the hydrophilic quinic-acid

moiety remained far from the surface and was exposed to water. The inset of Fig. 1d illustrates the structure of the CA-PDMS complex in the bound state, where the cinnamic-acid moiety is parallel to the substrate. This adsorption may also be caused by the planarity of the cinnamic-acid moiety, which minimises the solvent-accessible surface area and maximises the dispersion interactions with the equally planar PDMS surface.

3.5. Mechanical performance

It could be seen from Fig. S4 that CA-modification did not appreciably alter the mechanical properties of the PDMS. The Young's modulus, which was determined from the slope of the initial
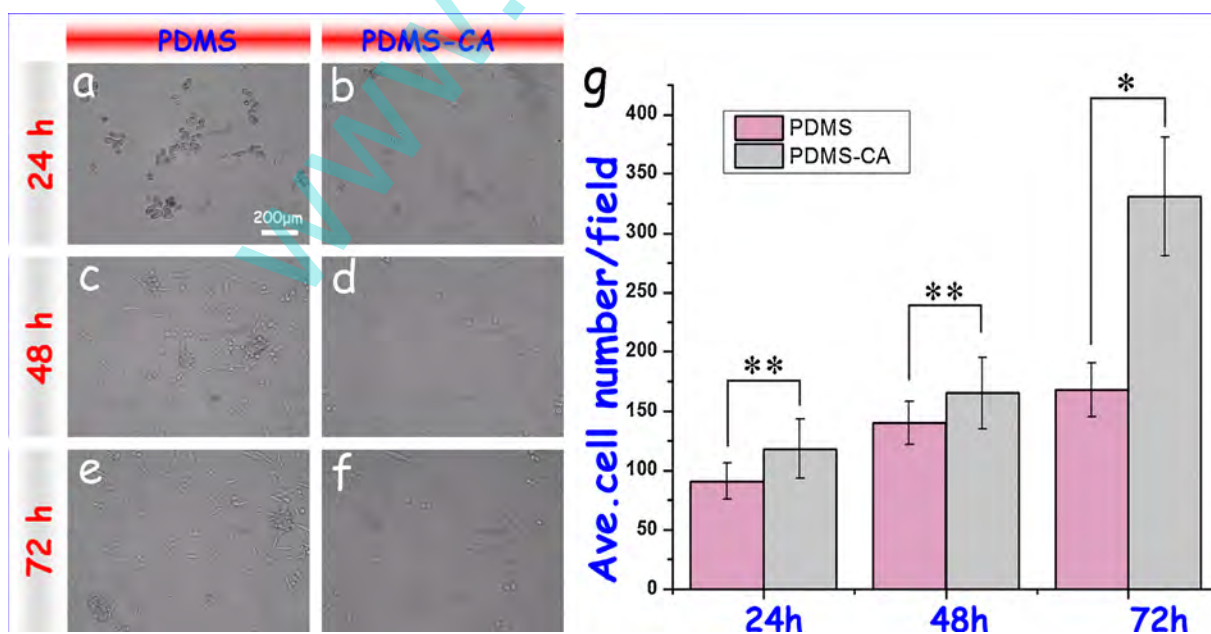

Fig. 3. Microscope images of HeLa cells cultured on PDMS surfaces: (a, c and e) nontreated PDMS substrate surfaces; (b, d and f) CA-modified PDMS surfaces; and (g) cell number per unit area (mean ± SD, $n = 6$, *: $p < 0.05$ and **: $p < 0.01$, compared with uncoated PDMS, Student's *t*-test). The scale bars are 200 μm.

linear portion of the stress-strain curve (Fig. S6), increased from 9.3 kPa to 9.7 kPa without significant difference. This might be attributed to stable chemical properties of PDMS. Also, these results were consistent with molecular modelling, which showed that the modification was predominately driven by van der Waals and electrostatic interactions.

3.6. Antimicrobial behaviour

The inhibitory activity of the CA modification was determined by comparing the viability of bacterial cells on modified PDMS membranes to unmodified PDMS membranes. As shown in Fig. 2, live bacteria express green fluorescent protein, whereas dead cells produce red fluorescence after incubation with PI. *E. coli* growth was inhibited and a greater quantity of dead cells (Fig. 3c and d) were observed on CA-modified PDMS membranes compared with bare PDMS membranes (Fig. 2a and b). We found that the inactivated rate increased from 14% to 70% after 2 h exposure to CA-coated PDMS, as shown in Fig. 3e. We conclude that bacterial growth was inhibited on the CA-coated PDMS substrate.

3.7. Cell morphology

Fig. 3 presents micrographs of the adhesion and proliferation of HeLa cells on the PDMS surfaces at three time points. Cells seeded on CA-coated PDMS were more spread with a flat morphology (Fig. 3b), whereas those on untreated PDMS displayed rounded morphologies after 24 h (Fig. 3a). Analogously, at both 48 h and 72 h, cells on the CA-coated surface were more spread and displayed healthier growth than those on the untreated surface. These intriguing results imply that CA can be an effective biomolecule for cell adhesion. Moreover, cell proliferation on surface-modified PDMS film was evaluated by cell counting. Fig. 3g shows the average number of cells in each field of view on the PDMS surfaces at three different time points. At 24 h, we found that the number of cells on the CA-coated film (about 100 cells/field) was higher than those on the untreated surfaces (about 80 cells/field). In the control group, approximately 120 cells were observed at 48 h, whereas in the CA-coated group approximately 150 cells were counted. This difference was greater at 72 h than at 48 h. These results suggest that CA can increase cell proliferation on PDMS surfaces.

4. Conclusions

In this study, a multifunctional PDMS substrate with antimicrobial properties that supports cell growth was prepared using a facile approach. The WCA results demonstrate that the wettability of the PDMS surface, which was initially hydrophobic, became slightly hydrophilic after CA modification. AFM showed that the roughness of the PDMS increased with CA coating. XPS confirmed that the CA-coated substrate was stable. The PMF of CA adsorption and additional MD simulations indicate that the cinnamic-acid moiety tended to adhere closely to the PDMS surface, whereas the quinic-acid moiety remained far from the surface and interacted with the solvent. Partitioning of the free-energy landscape suggests that van der Waals and electrostatic forces cooperatively drove the modification. Additionally, the CA-coated surface demonstrated antimicrobial properties. The cell culture experiments showed enhanced cell adhesion, spreading and growth on the CA-modified PDMS substrate, which confirmed the biocompatibility of the surface. Compared with other methods, the method presented here is facile, inexpensive, multifunctional and environmentally safe. Additionally, the proposed method is a general approach that can be applied to produce anti-bacterial surfaces on different substrates, such as PLGA and metallic devices. Given these advantages, this

approach may be a promising method for future studies on antimicrobial surfaces. We also expect that CA-coated materials will be used in biomedical devices and implants.

Appendix A. Supplementary data

Supplementary data associated with this article can be found, in the online version, at http://dx.doi.org/10.1016/j.colsurfb. 2013.11.010.

References

[1] M.S. Sumitha, K.T. Shalumon, V.N. Sreeja, R. Jayakumar, S.V. Nair, D. Menon, Biocompatible and antibacterial nanofibrous poly(ε-caprolactone)-nanosilver composite scaffolds for tissue engineering applications, Journal of Macromolecular Science: Part A 49 (2012) 131–138.
[2] L.G. Harris, R.G. Richards, Staphylococci and implant surfaces: a review, Injury 37 (2006) S3–S14.
[3] F. von Nussbaum, M. Brands, B. Hinzen, S. Weigand, D. Häbich, Antibacterial natural products in medicinal chemistry – exodus or revival? Angewandte Chemie International Edition 45 (2006) 5072–5129.
[4] D. Yong, M.A. Toleman, C.G. Giske, H.S. Cho, K. Sundman, K. Lee, T.R. Walsh, Characterization of a new metallo-β-lactamase gene, blaNDM-1, and a novel erythromycin esterase gene carried on a unique genetic structure in *Klebsiella pneumoniae* sequence type 14 from India, Antimicrobial Agents and Chemotherapy 53 (2009) 5046–5054.
[5] N.A. Rakow, K.S. Suslick, A colorimetric sensor array for odour visualization, Nature 406 (2000) 710–713.
[6] D.M. Eby, H.R. Luckarift, G.R. Johnson, Hybrid antimicrobial enzyme and silver nanoparticle coatings for medical instruments, ACS Applied Materials & Interfaces 1 (2009) 1553–1560.
[7] S. Chernousova, M. Epple, Silver as antibacterial agent: ion, nanoparticle, and metal, Angewandte Chemie International Edition 52 (2013) 1636–1653.
[8] M. Pollini, F. Paladini, A. Licciulli, A. Maffezzoli, L. Nicolais, A. Sannino, Silver-coated wool yarns with durable antibacterial properties, Journal of Applied Polymer Science 125 (2012) 2239–2244.
[9] O. Bar-Ilan, R.M. Albrecht, V.E. Fako, D.Y. Furgeson, Toxicity assessments of multisized gold and silver nanoparticles in zebrafish embryos, Small 5 (2009) 1897–1910.
[10] Y. Liu, B. Liu, D. Feng, C. Gao, M. Wu, N. He, X. Yang, L. Li, X. Feng, A progressive approach on zebrafish toward sensitive evaluation of nanoparticles toxicity, Integrative Biology-UK 4 (2012) 285–291.
[11] F. Gottschalk, B. Nowack, The release of engineered nanomaterials to the environment, Journal of Environmental Monitoring 13 (2011) 1145–1155.
[12] M.N. Clifford, Chlorogenic acids and other cinnamates – nature, occurrence and dietary burden, Journal of the Science of Food and Agriculture 79 (1999) 362–372.
[13] H. Ravn, L. Brimer, Structure and antibacterial activity of plantamajoside, a caffeic acid sugar ester from *Plantago major* subs *major*, Phytochemistry 27 (1988) 3433–3437.
[14] J.N. Lee, C. Park, G.M. Whitesides, Solvent compatibility of poly(dimethylsiloxane)-based microfluidic devices, Analytical Chemistry 75 (2003) 6544–6554.
[15] A. Komaromy, R.I. Boysen, H. Zhang, M.T.W. Hearn, D.V. Nicolau, Effect of various artificial surfaces on the colonization and viability of *E. coli* and *S. aureus*, BioMEMS and Nanotechnology III 6799 (2008) U125–U134.
[16] A. Goyal, A. Kumar, P.K. Patra, S. Mahendra, S. Tabatabaei, P.J.J. Alvarez, G. John, P.M. Ajayan, In situ synthesis of metal nanoparticle embedded free standing multifunctional PDMS films, Macromolecular Rapid Communications 30 (2009) 1116–1122.
[17] H.M.L. Tan, H. Fukuda, T. Akagi, T. Ichiki, Surface modification of poly(dimethylsiloxane) for controlling biological cells' adhesion using a scanning radical microjet, Thin Solid Films 515 (2007) 5172–5178.
[18] K. Efimenko, W.E. Wallace, J. Genzer, Surface modification of Sylgard-184 poly(dimethyl siloxane) networks by ultraviolet and ultraviolet/ozone treatment, Journal of Colloid and Interface Science 254 (2002) 306–315.
[19] Y. Liu, J.C. Fanguy, J.M. Bledsoe, C.S. Henry, Dynamic coating using polyelectrolyte multilayers for chemical control of electroosmotic flow in capillary electrophoresis microchips, Analytical Chemistry 72 (2000) 5939–5944.
[20] Y.H. Yan, M.B. Chan-Park, C.Y. Yue, CF4 plasma treatment of poly(dimethylsiloxane): effect of fillers and its application to high-aspect-ratio UV embossing, Langmuir 21 (2005) 8905–8912.

[21] G.A. Diaz-Quijada, D.D.M. Wayner, A simple approach to micropatterning and surface modification of poly(dimethylsiloxane), Langmuir 20 (2004) 9607–9611.

[22] A.W. Schuttelkopf, D.M.F. van Aalten, PRODRG: a tool for high-throughput crystallography of protein–ligand complexes, Acta Crystallographica Section D 60 (2004) 1355–1363.

[23] S.K. Baskaran, N. Goswami, S. Selvaraj, V.S. Muthusamy, B.S. Lakshmi, Molecular dynamics approach to probe the allosteric inhibition of PTP1B by chlorogenic and cichoric acid, Journal of Chemical Information and Modeling 52 (2012) 2004–2012.

[24] C.-Y. Gao, Y.-Y. Guo, J. He, M. Wu, Y. Liu, Z.-L. Chen, W.-S. Cai, Y.-L. Yang, C. Wang, X.-Z. Feng, L-3,4-dihydroxyphenylalanine-collagen modified PDMS surface for controlled cell culture, Journal of Materials Chemistry 22 (2012) 10763–10770.

[25] J.C. Phillips, R. Braun, W. Wang, J. Gumbart, E. Tajkhorshid, E. Villa, C. Chipot, R.D. Skeel, L. Kalé, K. Schulten, Scalable molecular dynamics with NAMD, Journal of Computational Chemistry 26 (2005) 1781–1802.

[26] I. Bahar, I. Zuniga, R. Dodge, W.L. Mattice, Conformational statistics of poly(dimethylsiloxane). 1. Probability distribution of rotational isomers from molecular dynamics simulations, Macromolecules 24 (1991) 2986–2992.

[27] J.S. Smith, O. Borodin, G.D. Smith, A quantum chemistry based force field for poly(dimethylsiloxane), The Journal of Physical Chemistry B 108 (2004) 20340–20350.

[28] W.L. Jorgensen, J. Chandrasekhar, J.D. Madura, R.W. Impey, M.L. Klein, Comparison of simple potential functions for simulating liquid water, The Journal of Chemical Physics 79 (1983) 926–935.

[29] T. Darden, D. York, L. Pedersen, Particle mesh Ewald: an N [center-dot] log(N) method for Ewald sums in large systems, The Journal of Chemical Physics 98 (1993) 10089–10092.

[30] S.E. Feller, Y. Zhang, R.W. Pastor, B.R. Brooks, Constant pressure molecular dynamics simulation: the Langevin piston method, The Journal of Chemical Physics 103 (1995) 4613–4621.

[31] J.-P. Ryckaert, G. Ciccotti, H.J.C. Berendsen, Numerical integration of the cartesian equations of motion of a system with constraints: molecular dynamics of *n*-alkanes, Journal of Computational Physics 23 (1977) 327–341.

[32] H.C. Andersen, Rattle: a velocity version of the shake algorithm for molecular dynamics calculations, Journal of Computational Physics 52 (1983) 24–34.

[33] W. Humphrey, A. Dalke, K. Schulten, VMD. Visual molecular dynamics, Journal of Molecular Graphics 14 (1996) 33–38.

[34] D. Trzesniak, A.-P.E. Kunz, W.F. van Gunsteren, A comparison of methods to compute the potential of mean force, ChemPhysChem: A European Journal of Chemical Physics and Physical Chemistry 8 (2007) 162–169.

[35] M. Hoefling, F. Iori, S. Corni, K.-E. Gottschalk, Interaction of amino acids with the Au(1 1 1) surface: adsorption free energies from molecular dynamics simulations, Langmuir 26 (2010) 8347–8351.

[36] L.B. Wright, T.R. Walsh, Facet selectivity of binding on quartz surfaces: free energy calculations of amino-acid analogue adsorption, The Journal of Physical Chemistry C 116 (2011) 2933–2945.

[37] E. Darve, A. Pohorille, Calculating free energies using average force, The Journal of Chemical Physics 115 (2001) 9169–9183.

[38] E. Darve, D. Rodriguez-Gomez, A. Pohorille, Adaptive biasing force method for scalar and vector free energy calculations, The Journal of Chemical Physics 128 (2008) 144120.

[39] J. Henin, C. Chipot, Overcoming free energy barriers using unconstrained molecular dynamics simulations, The Journal of Chemical Physics 121 (2004) 2904–2914.

[40] D. Rodriguez-Gomez, E. Darve, A. Pohorille, Assessing the efficiency of free energy calculation methods, The Journal of Chemical Physics 120 (2004) 3563–3578.

[41] C. Chipot, J. Henin, Exploring the free-energy landscape of a short peptide using an average force, The Journal of Chemical Physics 123 (2005) 244906.

[42] C. Depagne, S. Masse, T. Link, T. Coradin, Bacteria survival and growth in multi-layered silica thin films, Journal of Materials Chemistry 22 (2012) 12457–12460.

[43] C.J. Wilson, R.E. Clegg, D.I. Leavesley, M.J. Pearcy, Mediation of biomaterial–cell interactions by adsorbed proteins: a review, Tissue Engineering 11 (2005) 1–18.

[44] R.N. Wenzel, Surface roughness and contact angle, The Journal of Physical and Colloid Chemistry 53 (1948) 1466–1467.

[45] A.V. Singh, V. Vyas, R. Patil, V. Sharma, P.E. Scopelliti, G. Bongiorno, A. Podestà, C. Lenardi, W.N. Gade, P. Milani, Quantitative characterization of the influence of the nanoscale morphology of nanostructured surfaces on bacterial adhesion and biofilm formation, PLoS ONE 6 (2011) e25029.

[46] T.W. Chung, D.Z. Liu, S.Y. Wang, S.S. Wang, Enhancement of the growth of human endothelial cells by surface roughness at nanometer scale, Biomaterials 24 (2003) 4655–4661.